










# Tribological Characterization of Phosphate Coatings Deposited on Ti6Al4V

Diana-Petronela Burduhos-Nergis , Andrei Victor Sandu ,  
Dumitru-Doru Burduhos-Nergis , Nicanor Cimpoesu , Marcelin Benchea ,  
Mihai Popa , and Costica Bejinariu 

“Gheorghe Asachi” Technical University of Iasi, 41 “D. Mangeron” Street, 700050 Iasi, Romania  
sav@tuiasi.ro, costica.bejinariu@yahoo.com

**Abstract.** In recent years, improving the surface of titanium implants is increasingly being studied, in order to reduce their rejection rate. Thus, there are several methods by which the properties of the base material, in this case, the titanium alloy, can be improved, such as anodizing, micro-arc oxidation, plasma spraying, physical vapour deposition, biomimetic deposition, chemical conversion deposition etc. Regarding the deposition process by chemical conversion, the phosphating process presents a multitude of advantages, including good adhesion to the substrate and the capacity of improving cellular adhesion due to the porosity of the layer. Therefore, the paper aims to study the tribological characteristics by evaluating the adhesion and coefficient of friction of three types of phosphate layers deposited on the surface of the titanium alloy, Ti6Al4V, using a UMTR 2M-CTR Micro-tribometer and SEM. The results of the scratch tests revealed that the phosphate layers have good adhesion to the substrate and the values of the coefficient of friction were increased due to the roughness of the surface.

**Keywords:** Tribological characterization · Titanium · Phosphate layers

## 1 Introduction

Researchers' interest in bioengineering has expanded as a result of the accelerated expansion in demand for orthopaedic implants. Metallic materials, such as titanium alloys, stainless steel, and Co-Cr alloys, have long been employed in medical applications. Among these, titanium and its alloys, particularly Ti6Al4V, are the most often utilized biomaterials for the production of orthopaedic implants. The latter offers a variety of benefits, including good biocompatibility, low density, adequate corrosion and wear resistance, etc. The biggest drawback of Ti6Al4V titanium alloy, according to Pesode and Barve [1], is that it cannot interact with human bone because of its bio-inert surface, which can result in implant failure. Multiple studies [2–4] mentioned the likelihood of aluminium or vanadium being absorbed by the human body. This will have negative effects on the human body [5].

To find a solution to these identified problems, several researchers have tried to modify the surface characteristics of titanium and its alloys by depositing layers on the

metal surface [6–9]. Thus, one of the most studied types of coatings is the deposition of hydroxyapatite, by different processes such as electrochemical deposition [10], physical vapor deposition (PVD), sol-gel method [11] etc. Regarding the tribological characteristics, it was observed that the deposited layer has good resistance to the pressure of the blade, but its adhesion to the substrate is lower compared to those deposited by the chemical conversion process [5, 12].

Sovak [13] studied the osseointegration of Ti6Al4V after its coating with TiN coating, observing as a disadvantage a low adhesion of the layer to the substrate. Also, Qin [14] analyzed the improvements in the antibacterial and wear characteristics of Ti6Al4V after the deposition of a composite layer on the metal surface. The authors observed that the coefficient of friction decreased significantly and the antibacterial and cytocompatibility are good.

Recently, much attention has been paid to coatings on biometals surfaces deposited by a chemical conversion process called phosphating [15, 16]. The advantages of this method are highlighted in many studies, the most significant being: the promotion of osseointegration, the low cost of the deposition process, the enhancement of corrosion and wear resistance etc. [17, 18]. In addition, the deposited layers show high adhesion to the substrate due to the chemical conversion reactions between the metal and the phosphating solution [19].

Regarding the deposition of phosphate layers on titanium or its alloys, three types of coatings based on zinc, strontium, zinc-strontium, and zinc-calcium are known [17, 20, 21], depending on the nature of the metal ion in the phosphating solution. So, one of the novelties of this work is the use of three types of phosphate solutions. Two are completely original, based on zinc-magnesium and zinc-zirconium. The third one is based on zinc-calcium but with different activators and inhibitors. Over time, it has been observed that the bonding strength between the base material and the phosphate layer is influenced by the surface roughness, the activation process, the morphology of the coating, etc. [16].

Solanke [22] tested from the point of view of wear resistance several metal biomaterials, including Ti6Al4V, thus concluding that of all those tested, the titanium alloy is one of the most suitable for medical implants, however, considering that it is essential to use a surface coating. Even if the mechanical properties of the Ti6Al4V alloy have been analyzed, it is also necessary to analyze the tribological characteristics of the layers formed on its surface. Thus, this work studies the possibility of promoting cell adhesion and enhancing the surface properties of the titanium alloy. This is done by depositing new phosphate layers deposited by the chemical conversion process (phosphating). In this case, adhesion, coefficient of friction and surface scratch behaviour are studied for three different phosphate layers based on Mg-Zn, Zr-Zn, and Ca-Zn and also for the Ti6Al4V uncoated sample.

## 2 Materials and Methods

### 2.1 Material

The material used as the substrate for the deposition is Ti6Al4V, which was purchased from AEMMetal (Hunan, China). Its chemical composition according to the supplier is shown in Table 1.

**Table 1.** The chemical composition of Ti6Al4V.

| Element | Titanium | Aluminium | Vanadium | Iron | Oxygen | Carbon |
|---------|----------|-----------|----------|------|--------|--------|
| wt, %   | balance  | 6.14      | 4.22     | 0.12 | 0.11   | 0.03   |

### 2.2 Phosphating Process

Before the phosphating process, the bars were cut into 10x10x55 mm square samples. After this, the samples were sanded up to 1200 grit to obtain a homogeneous surface.

The steps involved in the phosphating process are shown in Fig. 1. The process starts with the degreasing of the samples by washing them, for 10 min, in an ultrasonic cleaner, by immersing them subsequently in three different media: technical acetone, ethanol, and distilled water. The second stage of the process is the removal of oxides and the activation of the surface. This is done by immersing for 15 s in a 2% HF solution and for 30 s in a titanium colloidal solution, at room temperature. During the third stage, the layer is obtained by immersing the samples in the phosphating solution for 60 min at 90 °C. In this paper, three different phosphating solutions based on zinc-magnesium, zinc-zirconium, and zinc-calcium were used. The phosphating solutions are a mixture of nitric acid, orthophosphoric acid, iron powder, sodium tripolyphosphate,

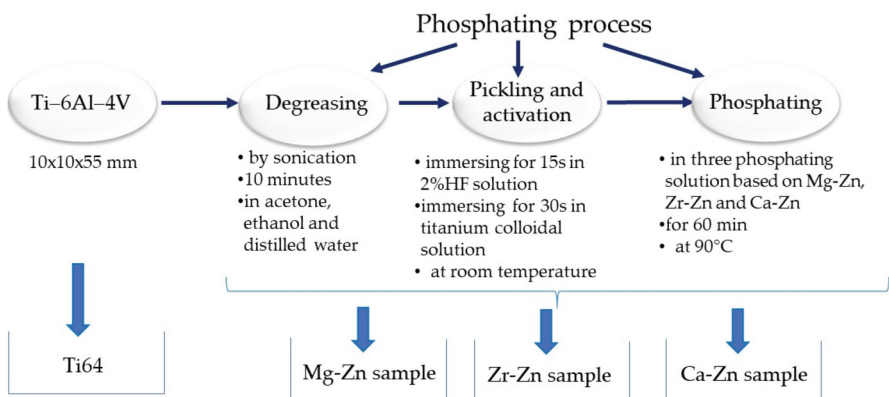


**Fig. 1.** The flow of the phosphating process and the types of samples obtained.

sodium hydroxide, sodium nitrite, sodium fluoride, zinc, and, depending on the type of solution, magnesium carbonate, zirconium oxide, or calcium nitride.

In order to be easier to understand, was used the following abbreviations:

Ti64 – for Ti6Al4V uncoated;

Mg-Zn – for the samples coated with a magnesium-zinc phosphate layer;

Zr-Zn – for the samples coated with a zirconium-zinc phosphate layer;

Ca-Zn – for the samples coated with a calcium-zinc phosphate layer.

### 2.3 Characterization Methods

A scanning electron microscope (Vega Tescan LMH II), equipped with Energy-dispersive X-ray spectroscopy (EDX) analysis equipment was used to examine the morphology and scratch traces of the samples.

Scratch tests were performed using a UMTR 2M-CTR Micro-tribometer. The scratch test settings are as follows: the distance covered by the blade is 10 mm, the blade speed is 167  $\mu\text{m}/\text{second}$ , and the normal force grows with time from 0 to 10N. Using this test, the layer was gradually removed from the Ti6Al4V surface. This test examines the parameters described further:  $F_x$ , which is the response force value,  $F_z$ , which is the normal load force,  $F_f$  which is the friction force, COF, which is the coefficient of friction and AE which is acoustic emission.

## 3 Results and Discussions

**The Ti6Al4V uncoated sample.** The Ti64 sample presents an approximately constant value with small variations of the coefficient of friction due to its homogeneous surface, as can be observed in Fig. 2.

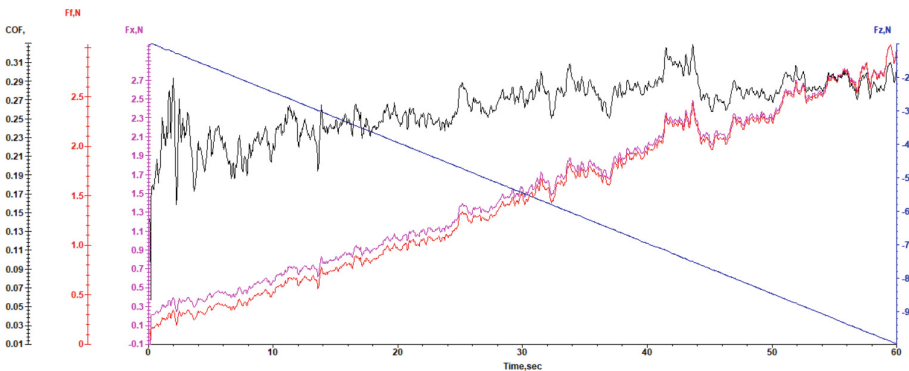


**Fig. 2.** Time variation of  $F_x$ ,  $F_z$ ,  $F_f$  and COF during the scratch test for the Ti64 sample.

In this case the average value of the coefficient of friction was close to 0.26 value, with a standard deviation (std) of 0.03. Between 40–45 s can be observed that it is a significant increase in the values of COF close to the 3 N, followed by a decrease of

the  $F_x$  value. This can be explained by the material that was blocked in the front of the blade. Also, the average value of  $F_f$  is close to 2.21, with a std of 0.09. Furthermore, as can be seen from Fig. 3, the acoustic emission is decreasing after the COF has stabilized, its average value being close to 0.07 with a std of 0.003. These values are influenced by the mechanical preparation of the surface, this one being grinding at 800 grids.

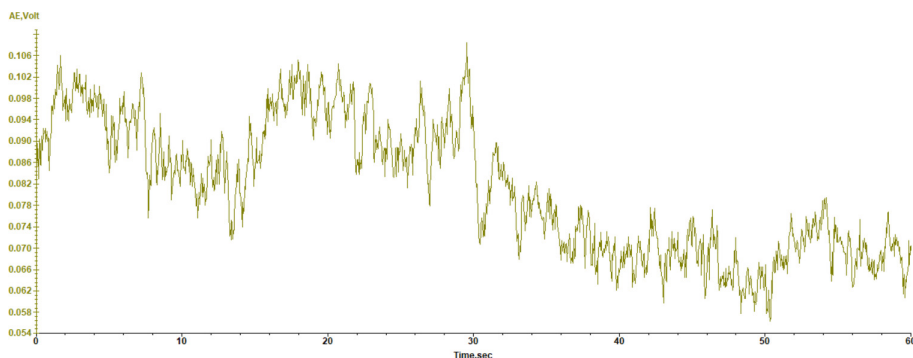


**Fig. 3.** Time variation of AE during the scratch test for the Ti64 sample.

The microstructural analysis of the scratch and the trace profile are presented in Figs. 4a and 4c. Also, in Fig. 4b and the 3D profile (Fig. 4d) can be observed close to the end of the scratch, the material parts stuck.

**The Mg-Zn sample.** After deposition of the magnesium-zinc phosphate layer on the Ti6Al4V alloy surface, the average value of the coefficient of friction almost doubles to 0.48, with a std of 0.09. Close to 25 s, the slope of the COF and  $F_f$  is changing, probably due to the cracking of the phosphate crystals (Fig. 5), close to a load value of 3 N. The fluctuation of the COF values is related to the roughness of the phosphate layer, which has a value of 2.21  $\mu\text{m}$ . The AE presented in Fig. 6 shows a constant profile, with small variations which are probably appearing due to the crystal's cracks. The AE average value is 0.002 with a std of 0.002.

The SEM analysis of the Mg-Zn phosphate layer deposited on the Ti6Al4V surface shows crystals specific to the phosphate layer based on Zn, which were partially removed from the titanium alloy surface, close to the final part of the scratch (Fig. 7a). This aspect can be observed, also, in Fig. 7b, where can be seen parts of the crystals on the scratch track. The roughness of the surface is visible in Figs. 7c and 7d. The elemental mapping shows the end of the scratch track. As can be seen from Fig. 8, due to the fact that the layer was obtained by a chemical conversion process, the presence of the principal elements of the layer (Zn, Mg, Fe, P and O) can be observed, but in small quantities compared with the edges. Also, at this moment, a big part of the layer was removed and the quantity of Ti in that zone was increased.

**The Zr-Zn sample.** The scratching behaviour of the Zr-Zn sample is different from that of the Mg-Zn solution phosphate sample (Fig. 9). Thus, a sudden increase in the coefficient of friction can be observed, which corresponds to a load force of 4.7 N, close to 22 s. The mean value of COF is 0.34, with a std of 0.12, while the mean value of  $F_f$  is

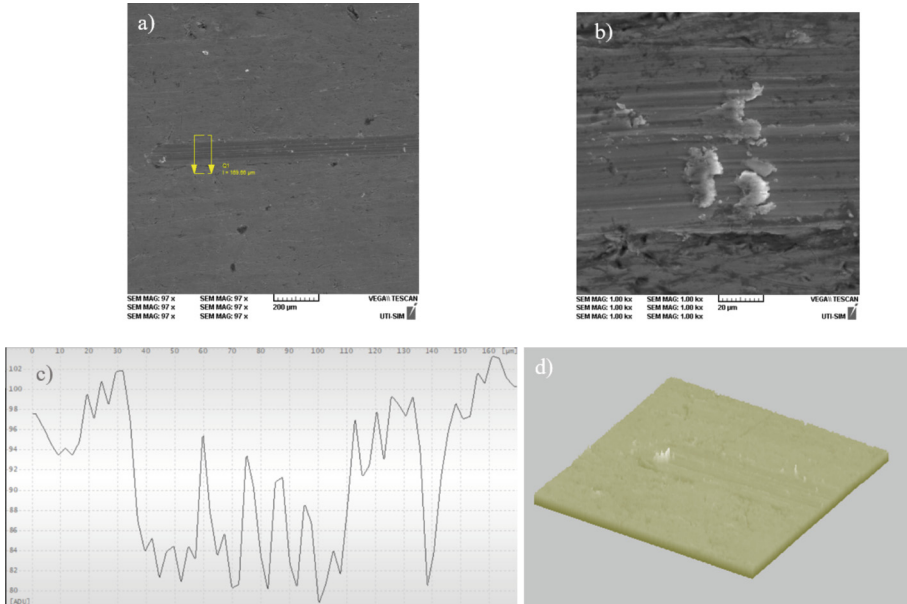


**Fig. 4.** Ti64 microstructure after scratch test a) SEM morphology of the trace 250x; b) SEM image of stuck material 1kx; c) scratch profile; d) 3D profile.

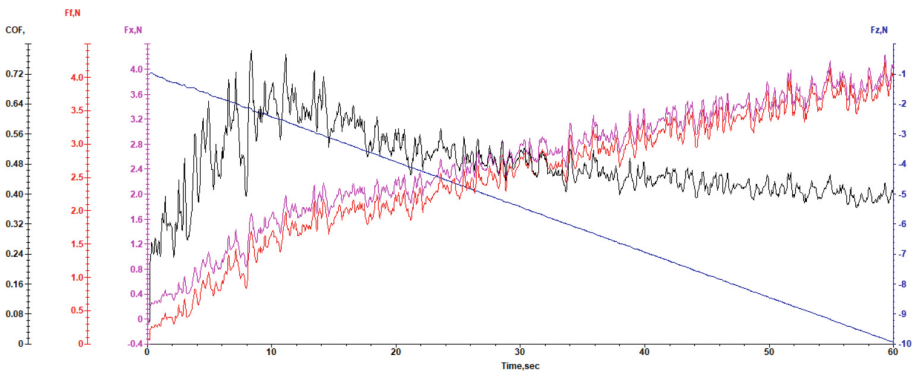


**Fig. 5.** Time variation of  $F_x$ ,  $F_z$ ,  $F_f$  and COF during the scratch test for the Mg-Zn sample.

2.07 N, with a std of 1.26. Compared to the Mg-Zn phosphate-coated sample, the Zr-Zn sample has a much lower roughness value, approximately  $0.96 \mu\text{m}$ , thus explaining the lower values of COF and  $F_f$ . The same change close to 22 s can be observed also in Fig. 10, where the AE curve presents variations after this time, probably due to different dimensions and positions of crystals which are cracking at contact with the blade. In this case, the AE average value is 0.003 with a std of 0.003.

The SEM images of the Zr-Zn phosphate layer show crystals specific to compounds formed on the surface of Ti6Al4V, especially of zinc phosphate tetrahydrate (Fig. 11a). In

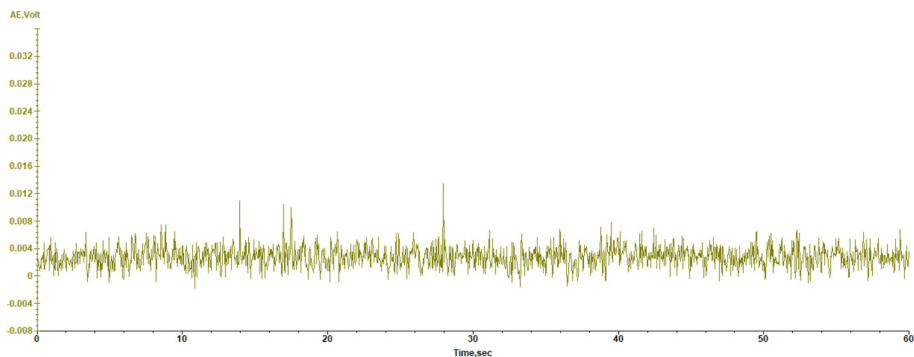


**Fig. 6.** Time variation of AE during the scratch test for the Mg-Zn sample.

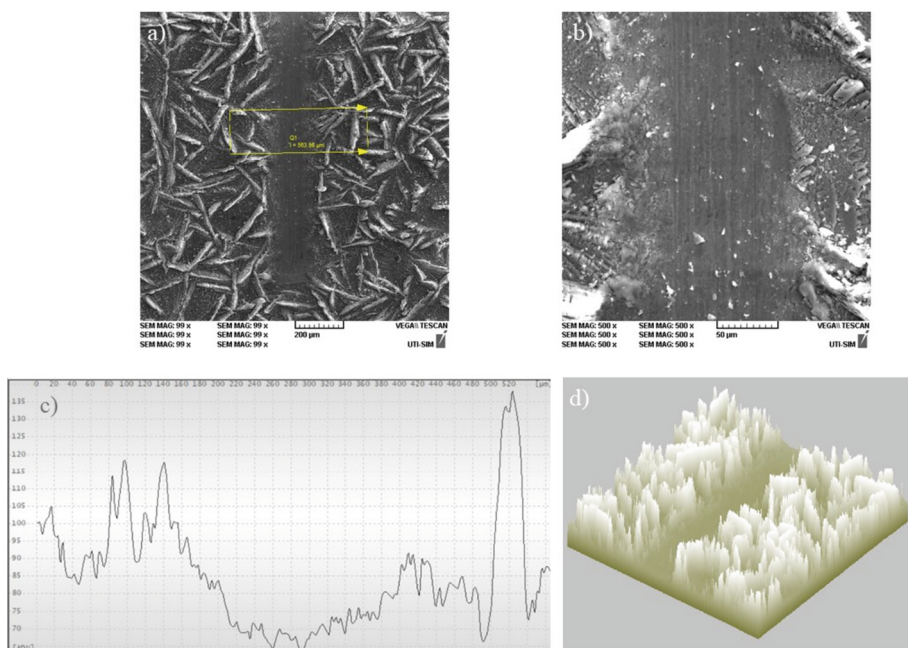


**Fig. 7.** Mg-Zn sample microstructure after scratch test a) SEM morphology of the trace 100x; b) SEM morphology with crack crystals 500x; c) scratch profile; d) 3D profile.

this case, compared with the Mg-Zn sample, the phosphate crystals are denser, covering the entire surface of the sample (Fig. 11b). Also, can be observed that the intercrystalline zones are smaller compared with the Mg-Zn phosphate layer, which determines a lower roughness value (Figs. 11c and 11d). Moreover, can be observed that the phosphate layer was removed from the surface of Ti6Al4V, with only small parts of the crystals remaining. The EDX analysis determined the elemental mapping of the main elements of the layer at the end of the scratch (Fig. 12). As can be seen, the presents of Ti in



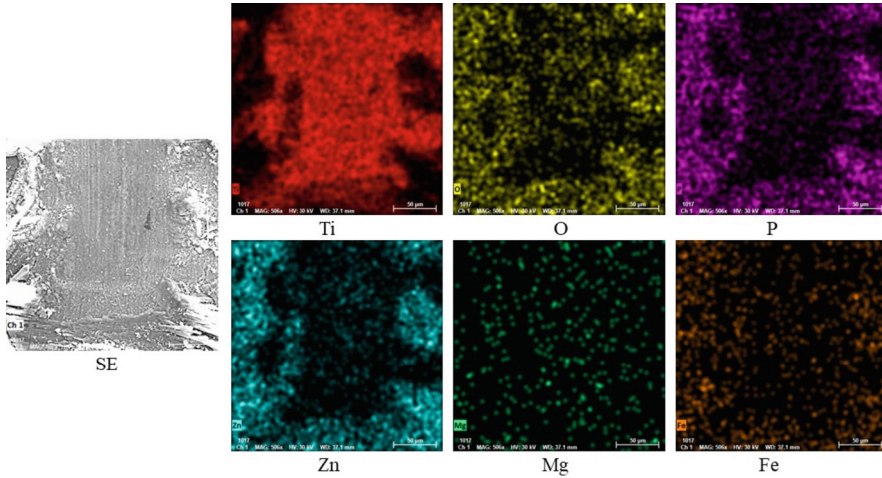


**Fig. 8.** The elemental mapping of the main elements of the Mg-Zn sample after the scratch test.

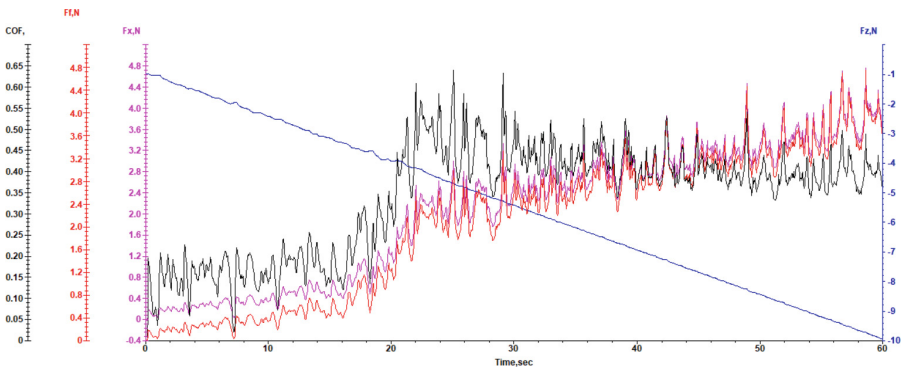


**Fig. 9.** Time variation of  $F_x$ ,  $F_z$ ,  $F_f$  and COF during the scratch test for the Zr-Zn sample.

high quantity indicates that the phosphate layer was partially removed, but taken into consideration that the phosphate layer was formed by chemical conversion process and just a small quantity of  $ZrO_2$  was used in the phosphating solution, the Zn, Zr, P, O and Fe can be detected on the track's blade.

**The Ca-Zn sample.** The sample on which was deposited a Ca-Zn phosphate layer shows similar scratching behaviour to the sample coated with an Mg-Zn layer, as can be seen in Fig. 13. At the same time, the average value of the friction coefficient is 0.47, with a std of 0.1, very close to the value of the Mg-Zn sample (0.48). This behaviour is also due to the specific roughness of the layer, amounting to  $1.34 \mu\text{m}$ . As can be observed in Fig. 13, close to 19 s the crystals started to yield under the pressure of the blade and the COF becomes almost constant, at a load force of 2.1 N. Also, the AE graphic presents many peaks which can be attributed to the failure of big



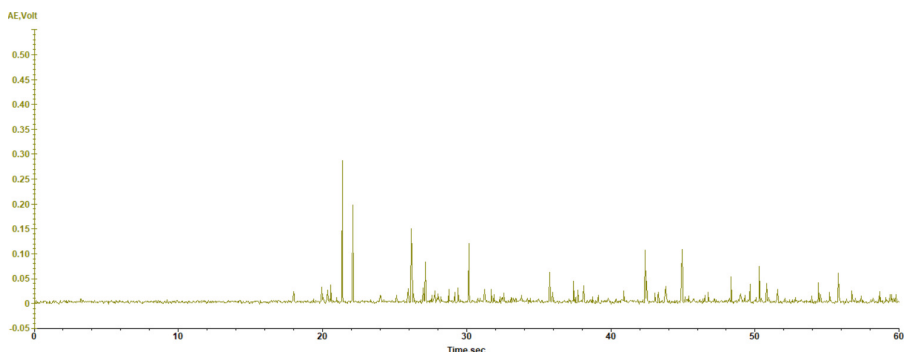


**Fig. 10.** Time variation of AE during the scratch test for the Zr-Zn sample.

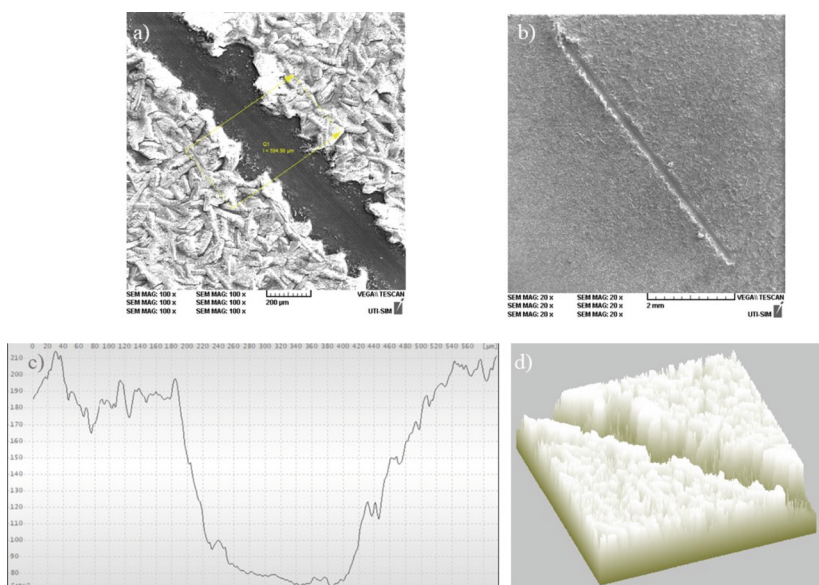


**Fig. 11.** Zr-Zn sample microstructure after scratch test a) SEM morphology of the trace 100x; b) SEM morphology with the entire scratch track 25x; c) scratch profile; d) 3D profile.

phosphate crystals at contact with the blade, the average AE value being 0.004 with a std of 0.002, Fig. 14.

The difference between the morphology of the Ca-Zn phosphate layer compared with the Zr-Zn and Mg-Zn layer can be observed in Figs. 15a and 15b. The biggest difference in structure is between the Zr-Zn and Ca-Zn layers, especially regarding the dimensions of the crystals, which are smaller for the Zr-Zn sample. The Ca-Zn layer also presents intercrystallite zones which are similar to the Mg-Zn sample structure. The presence of these zones and the dimension of crystals explain the value of roughness, which can be observed also in Figs. 15c and 15d. The elemental mapping of the main elements of the

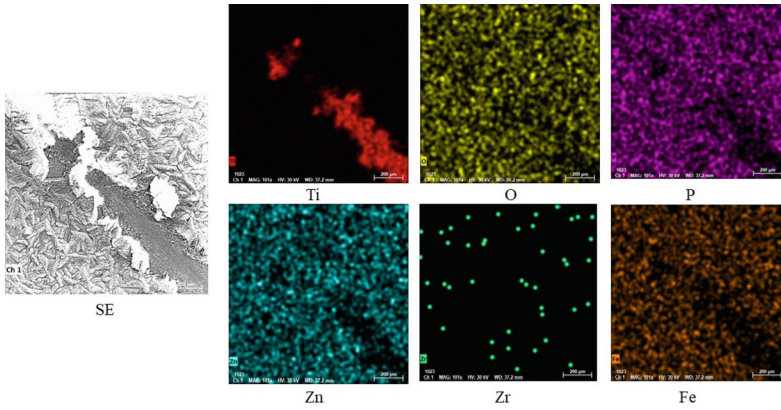


**Fig. 12.** The elemental mapping of the main elements of the Zr-Zn sample at the end of the scratch track.

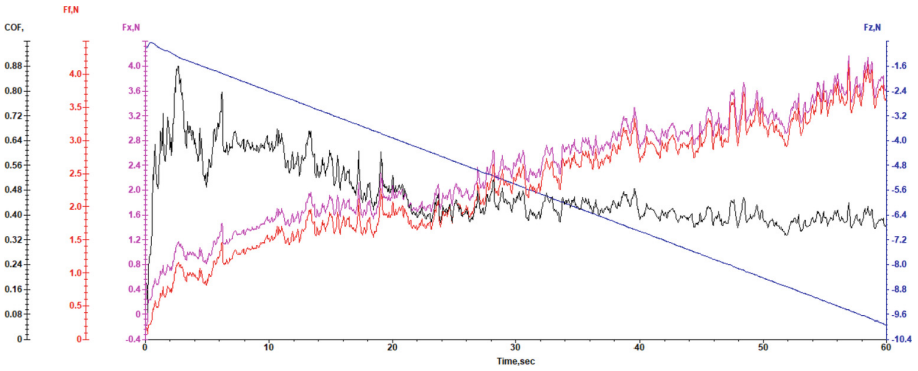


**Fig. 13.** Time variation of  $F_x$ ,  $F_z$ ,  $F_f$  and COF during the scratch test for the Ca-Zn sample.

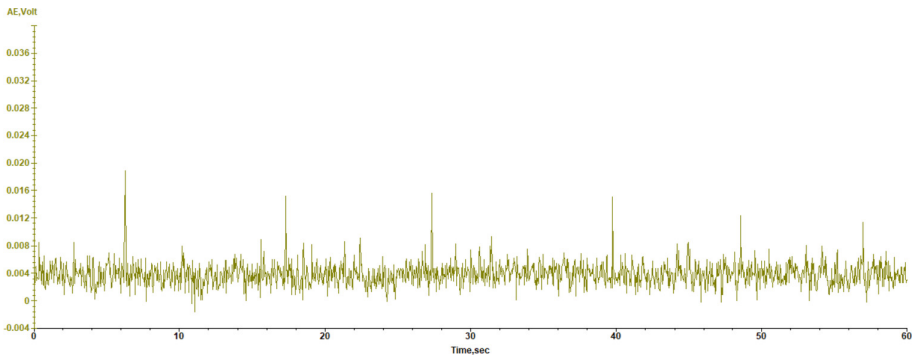


**Fig. 14.** Time variation of AE during the scratch test for the Ca-Zn sample.

Ca-Zn phosphate layer after the scratch test is presented in Fig. 16. As can be observed, the phosphate layer was removed partially, but as in other cases (Mg-Zn and Zr-Zn) some parts of the crystals remain on the surface of Ti6Al4V. Another important aspect is the big quantity of Ti, which indicates that in the intercrystalline zone, the layer of phosphate is very thin, being easier for the blade to remove the layer in those areas.

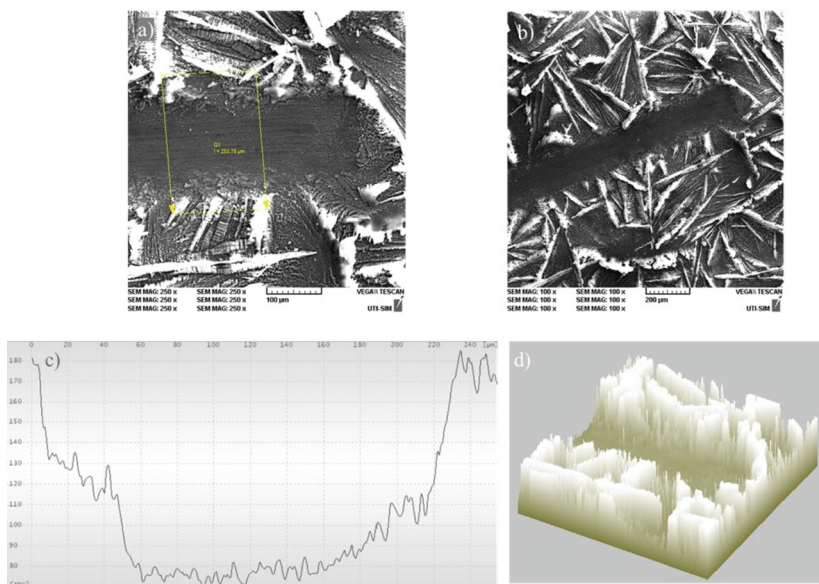


**Fig. 15.** Ca-Zn sample microstructure after scratch test; SEM morphologies of the trace a) 250x and b) 100x; c) scratch profile; d) 3D profile.

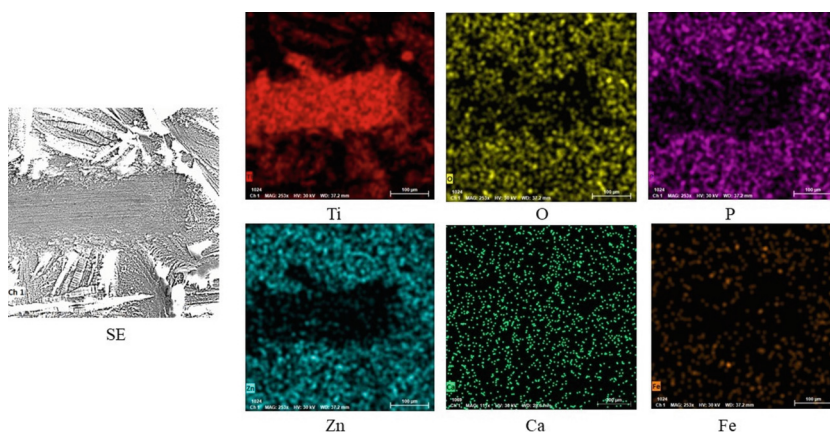


**Fig. 16.** The elemental mapping of the main elements of the Ca-Zn sample at the end of the scratch track.

## 4 Conclusions

To promote the surface characteristics of the Ti6Al4V alloy was deposited by chemical conversion process three different phosphate layers based on magnesium-zinc, zirconium-zinc and calcium-zinc. The tribological properties of the layers obtained and the uncoated sample were studied using the scratch method. Also, the scratch track was analyzed by SEM and EDX. After deposition, the roughness value of the surface obtained was increased considerably. Influenced by the roughness of the surface, the value of the coefficient of friction has doubled from 0.24 for the uncoated sample to 0.48 and 0.47 for Mg-Zn and Ca-Zn samples. From the coated samples, the one with the smallest roughness is the Zr-Zn sample, the SEM micrographs show that the layer is more compact. Also, the scratch test and EDX analysis revealed that this sample has the best adhesion to the substrate, even if the layer was not completely removed from the other samples either. Due to the modification of the surface characteristics by enhancing the roughness of the layer, can be concluded that the phosphate layer obtained on the surface of Ti6Al4V can promote cell adhesion.

**Acknowledgement.** This paper was realized with the support of COMPETE 2.0 project nr.27PFE/2021, financed by the Romanian Government, Minister of Research, Innovation and Digitalization. This paper was also supported by “Gheorghe Asachi” Technical University from Iași (TUIASI), through the Project “Performance and excellence in postdoctoral research 2022”.

## References

1. Pesode, P., Barve, S.: A review-metastable  $\beta$  titanium alloy for biomedical applications. *J. Eng. Appl. Sci.* **70**, 1–36 (2023)
2. Barchowsky, A.: Systemic and immune toxicity of implanted materials. *Biomaterials Science. An Introduction to Materials in Medicine*, 791–799 (2020)
3. Manivasagam, G., Dhinasekaran, D., Rajamanickam, A.: Biomedical implants: corrosion and its prevention - a review. *Recent Patents on Corrosion Science* **2**, 40–54 (2010)
4. Kim, K.T., Eo, M.Y., Nguyen, T.T.H., Kim, S.M.: General review of titanium toxicity. *Int. J. Implant Dentistry* **5**(1), 1–12 (2019)
5. Singh, G., Sharma, N., Kumar, D., Hegab, H.: Design, development and tribological characterization of Ti–6Al–4V/hydroxyapatite composite for bio-implant applications. *Mater. Chem. Phys.* **243**, 122662 (2020)
6. Neubauer, J.A.: Invited review: physiological and pathophysiological responses to intermittent hypoxia. *J. Appl. Physiol.* **90**, 1593–1599 (2001)
7. Priyadarshini, B., Rama, M., Chetan, Vijayalakshmi, U.: Bioactive coating as a surface modification technique for biocompatible metallic implants: a review. *J. Asian Ceramic Societies* **7**(1), 397406 (2019)
8. Kurup, A., Dhattrak, P., Khasnis, N.: Surface modification techniques of titanium and titanium alloys for biomedical dental applications: a review. *Mater Today Proc.* **39**, 84–90 (2021)
9. Zhao, L., Chu, P.K., Zhang, Y., Wu, Z.: Antibacterial coatings on titanium implants. *J. Biomed. Mater. Res. B Appl. Biomater.* **91B**, 470–480 (2009)
10. Mehrvarz, A., Khalil-Allafi, J., Khosrowshahi, A.K.: Biocompatibility and antibacterial behavior of electrochemically deposited Hydroxyapatite/ZnO porous nanocomposite on NiTi biomedical alloy. *Ceram. Int.* **48**, 16326–16336 (2022)

11. Choi, G., Choi, A.H., Evans, L.A., Akyol, S., Ben-Nissan, B.: A review: recent advances in sol-gel-derived hydroxyapatite nanocoatings for clinical applications. *J. Am. Ceram. Soc.* **103**, 5442–5453 (2020)
12. Behera, R.R., Das, A., Pamu, D., Pandey, L.M., Sankar, M.R.: Mechano-tribological properties and in vitro bioactivity of biphasic calcium phosphate coating on Ti-6Al-4V. *J. Mech. Behav. Biomed. Mater.* **86**, 143–157 (2018)
13. Sovak, G., Weiss, A., Gotman, I.: Osseointegration of Ti6Al4V alloy implants coated with titanium nitride by a new method. *J. Bone Joint Surg Br.* **82**(2), 290–296 (2000)
14. Qin, W., Ma, J., Liang, Q., Li, J., Tang, B.: Tribological, cytotoxicity and antibacterial properties of graphene oxide/carbon fibers/polyetheretherketone composite coatings on Ti-6Al-4V alloy as orthopedic/dental implants. *J. Mech. Behav. Biomed. Mater.* **122**, 104659 (2021)
15. Phuong, N.V., Lee, K., Chang, D., Kim, M., Lee, S., Moon, S.: Zinc phosphate conversion coatings on magnesium alloys: a review. *Met. Mater. Int.* **19**, 273–281 (2013)
16. Liu, B., Zhang, X., Xiao, G.Y., Lu, Y.P.: Phosphate chemical conversion coatings on metallic substrates for biomedical application: a review. *Mater. Sci. Eng. C* **47**, 97–104 (2015)
17. Liu, B., Shi, X.M., Xiao, G.Y., Lu, Y.P.: In-situ preparation of scholizite conversion coatings on titanium and Ti-6Al-4V for biomedical applications. *Colloids Surf B Biointerfaces* **153**, 291–299 (2017)
18. Zhao, D.W., et al.: Interleukin-4 assisted calcium-strontium-zinc-phosphate coating induces controllable macrophage polarization and promotes osseointegration on titanium implant. *Mater Sci Eng C Mater Biol Appl.* **118**, 111512 (2021)
19. Zuo, K.Q., et al.: Controllable phases evolution and properties of zinc-phosphate/strontium-zinc-phosphate composite conversion coatings on Ti: effect of temperature. *Surf Coat Technol.* **447**, 128885 (2022)
20. Zhao, D.W., et al.: Strontium-zinc phosphate chemical conversion coating improves the osseointegration of titanium implants by regulating macrophage polarization. *Chem. Eng. J.* **408**, 127362 (2021)
21. Liu, B., Xiao, G.Y., Chen, C.Z., Lu, Y.P., Geng, X.W.: Hopeite and scholizite coatings formation on titanium via wet-chemical conversion with controlled temperature. *Surf Coat Technol.* **384**, 125330 (2020)
22. Solanke, S., Gaval, V., Sanghavi, S.: In vitro tribological investigation and osseointegration assessment for metallic orthopedic bioimplant materials. *Mater Today Proc.* **44**, 4173–4178 (2021)